HHS Public Access

Author manuscript

J Neural Eng. Author manuscript; available in PMC 2017 December 12.

Published in final edited form as:

J Neural Eng. 2016 June ; 13(3): 036006. doi:10.1088/1741-2560/13/3/036006.

Gait adaptation to visual kinematic perturbations using a real-time closed-loop brain computer interface to a virtual reality avatar

Trieu Phat Luu, **Yongtian He**, **Samuel Brown**, **Sho Nakagame**, and **Jose L. Contreras-Vidal**

Noninvasive Brain-Machine Interface System Laboratory, Dept. of Electrical and Computer Engineering, University of Houston, Houston, TX 77004, USA

Abstract

Objective—The control of human bipedal locomotion is of great interest to the field of lower-body brain computer interfaces (BCIs) for gait rehabilitation. While the feasibility of closed-loop BCI systems for the control of a lower body exoskeleton has been recently shown, multi-day closed-loop neural decoding of human gait in a BCI virtual reality (BCI-VR) environment has yet to be demonstrated. BCI-VR systems provide valuable alternatives for movement rehabilitation when wearable robots are not desirable due to medical conditions, cost, accessibility, usability, or patient preferences.

Approach—In this study, we propose a real-time closed-loop BCI that decodes lower limb joint angles from scalp electroencephalography (EEG) during treadmill walking to control a walking avatar in a virtual environment. Fluctuations in the amplitude of slow cortical potentials of EEG in the delta band (0.1 – 3 Hz) were used for prediction; thus, the EEG features correspond to time-domain amplitude modulated (AM) potentials in the delta band. Virtual kinematic perturbations resulting in asymmetric walking gait patterns of the avatar were also introduced to investigate gait adaptation using the closed-loop BCI-VR system over a period of eight days.

Main results—Our results demonstrate the feasibility of using a closed-loop BCI to learn to control a walking avatar under normal and altered visuomotor perturbations, which involved cortical adaptations. The average decoding accuracies (Pearson's r values) in real-time BCI across all subjects increased from (Hip: 0.18 ± 0.31; Knee: 0.23 ± 0.33; Ankle: 0.14 ± 0.22) on Day 1 to (Hip: 0.40 ± 0.24; Knee: 0.55 ± 0.20; Ankle: 0.29 ± 0.22) on Day 8.

Significance—These findings have implications for the development of a real-time closed-loop EEG-based BCI-VR system for gait rehabilitation after stroke and for understanding cortical plasticity induced by a closed-loop BCI-VR system.

Keywords

Brain computer interfaces; visuomotor adaptation; gait adaptation; BCI-VR systems

Correspondence: Trieu Phat Luu, Department of Electrical and Computer Engineering, University of Houston, N308 Engineering Building 1, Houston, TX 77204, USA., ptluu2@central.uh.edu.

1.Introduction

Walking is a complex task, and its quality is usually determined by comparison to a smooth and symmetric walking gait pattern. However, patients with cerebral damage from stroke often adopt asymmetric walking patterns (Hsu et al., 2003, Lamontagne and Fung, 2004). Prior studies of gait adaptation to a split-belt perturbation, which creates asymmetric walking, demonstrated that temporal and spatial control for symmetric gait can be adapted separately (Malone et al., 2012). Moreover, the understanding of motor adaptation mechanisms may suggest appropriate interventions for gait rehabilitation. Analyses of aftereffects following split-belt treadmill adaptation showed that walking adaptation partially transfers to over-ground walking in patients post-stroke. This could imply that the persistence of improved symmetry can be used in gait restoration in post-stroke gait rehabilitation (Reisman et al., 2009).

Rehabilitation based on Virtual Reality or Virtual Environment (VR/VE) is an emergent area of research that provides several advantages to the patients and researchers (Bohil et al., 2011, Holden, 2005). VE creates an interactive environment that immerses the user in the experimental setting. This is important in rehabilitation to ensure patient's engagement and motivation to improve performance (Rizzo and Kim, 2005). Applications of VR/VE in rehabilitation are growing; for example, a VR soccer game was used to improve walking performance for pediatric rehabilitation (Brutsch et al., 2010). Another study showed the advantages of using VE in gait rehabilitation by creating an obstacle avoidance VE system during walking in chronic post-stroke patients (Jaffe et al., 2004). Moreover, there are a few randomized controlled trial (RCT) studies reported that VR could be beneficial for gait rehabilitation (Yang et al., 2008) and for improving balance in chronic stroke patients (Llorens et al., 2015). Interestingly, some research showed that a VR intervention is effective on triggering cortical reorganization and associated locomotor recovery (You et al., 2005).

Neural engineering approaches to the study and restoration of gait function have demonstrated the possibility of reconstructing gait kinematics from patterns of cortical activity acquired via intracortical electrode arrays in non-human primates (Fitzsimmons et al., 2009) and non-invasive scalp electroencephalography (EEG) in human subjects (Presacco et al., 2011) with the same accuracy, for a review see (Chéron et al., 2012). More recently, Bulea *et al.* decoded sit-to-stand and stand-to-sit movements from EEG signals recorded immediately prior to those actions suggesting EEG can be used to predict locomotive and non-locomotive actions (Bulea et al., 2014). Moreover, Kilicarslan *et al.* pioneered the deployment of EEG-based BCI systems to control lower-body powered robotic exoskeletons by subjects with spinal cord injury (SCI) (Kilicarslan et al., 2013). Applications of BCI systems for gait rehabilitation using VR/VE represent a new form of personalized neurorehabilitation based on putative shared brain networks involved in action observation and action execution (Morone et al., 2015, Hashimoto et al., 2010, Wang et al., 2012, King et al., 2013). Although these studies initially showed the possibility of deploying BCI-VR systems in rehabilitation, there are no gait studies that investigate visuomotor adaptation tasks and little is known about whether and how brain networks adapt during gait adaptation based on BCI-VR systems.

In this study, an EEG-based BCI-VR system based on the unscented Kalman filter (UKF) has been designed to infer, in real-time, lower limb joint angles during treadmill walking in healthy subjects. Fluctuations in the amplitude of slow cortical potentials of EEG in the delta band (0.1 – 3 Hz) were used for prediction; thus, the EEG features correspond to time-domain amplitude modulated potentials in the delta band. The predicted joint angles were used to control a walking avatar in a VE, thereby closing the loop through the brain. Virtual kinematic perturbations of subjects' walking patterns were also introduced to investigate the changes in brain activity to gait during adaptation using the closed-loop BCI-VR. The virtual kinematic perturbations resulted in an asymmetric walking pattern of the walking avatar. We hypothesized that, with practice, the subjects could gain better BCI control and reduce the gait asymmetry of the walking avatar through EEG signals. Motor imagery was not done in this study because 1) actual gait movements from subjects are known to lead to stronger neural signals than imagery alone, which are easier to decode (Yuan et al., 2010), and 2) the intended application is for gait rehabilitation after stroke where actual movement and degree of gait symmetry are critical variables for rehabilitation (Venkatakrishnan et al., 2014).

2.Materials and Methods

2.1.Experimental Setup and Procedure

Four healthy male subjects (ages from 23 to 27 years) with no history of neurological disease or lower limb pathology participated in this study. All participants provided informed consent as approved by the Institutional Review Board at the University of Houston. Each subject participated in eight sessions which were identical, but occurred on different days. Each session lasted for about 50 minutes (mins). Subjects were instructed to have 2 mins of standing still in the beginning and end of each session. In the remaining period, subjects walked on a treadmill at a fixed speed of 1 mile/hour (mph). A television monitor was placed in front of the treadmill, displaying an avatar of the subjects standing/walking in a virtual environment (VE) (Figure 2A). The screen only showed movement of body parts below the waist of the avatar, because this study focused on lower limb movements. The avatar followed the subject's lower limb movements precisely in real-time by matching the joint angles (hip, knee, and ankle) on both legs. Each joint angle (in the sagittal plane) was measured using goniometers. For safety purposes, all subjects were instructed to hold onto a front handle bar while walking on the treadmill, thus simulating a walker device.

As illustrated in Figure 1, each session began with the subject standing still on the treadmill for 2 mins. The treadmill was then slowly sped up to 1 mph, over approximately 20 seconds, by the experimenters. The subject was able to see the avatar following his/her movement correctly. In the first 15 mins, the walking avatar was controlled by signals from the goniometers (*gonio-control* phase). In this phase, the unscented Kalman filter and its parameters were trained and updated every min in the background. UKF's parameters were fixed at the end of this phase. A detailed description of this algorithm is provided in Section 2.4. The *gonio-control* phase was followed by an *EEG-control* phase, in which the lower limb joint angles of the avatar's right leg followed the outputs from the real-time BCI decoder instead of the goniometers. In both *gonio-* and *EEG-control* phases, the avatar's left

leg was driven from goniometer data. The *EEG-control* phase consists of three parts: pre-exposure (8 mins), exposure (15 mins), and post-exposure (8 mins). During the exposure period, a visual kinematic perturbation was introduced to the avatar: all joint angles on the avatar's right leg were linearly scaled down to 70% of the decoder outputs. The subject was instructed to think about controlling the avatar to walk normally while looking at the avatar. Meanwhile, the subject continued to walk on the treadmill during all phases. In the end, the session terminated after the subject had 2 mins of standing still on the treadmill.

2.2.Data Collection

Whole scalp 64-channel active EEG data were collected (ActiCap system, Brain Products GmbH, Germany) and labeled in accordance with the extended 10–20 international system. A wireless interface (MOVE system, Brain Products GmbH, Germany) was used to transmit data (sampled at 100 Hz) to the host PC. There was a small difference in arrangement of EEG channels between subjects. For the first 2 subjects, 64 EEG channels followed the standard setup (ground channel, GND, at FCz, and reference channel, REF, at AFz). There were some changes in the arrangement of EEG channels for the next two subjects: GND and REF were moved to the left and right earlobe (A1 and A2), respectively, four EEG channels (T7, T8, TP9 and TP10) were used as electrooculogram (EOG) to capture eye blinks and eye movements. The purpose of this modification is to improve the real-time decoding accuracies based on results found from our previous study (Luu et al., 2015). The two main reasons are: 1) GND and REF channels in the standard setup were very close to the motor cortex and 2) EOG sensors were required in our real-time artifact removal algorithm (details in Section 2.3).

Lower limb joint angles in sagittal plane were recorded by goniometers (SG150 & SG110/A Gonio electrodes, Biometrics Ltd, UK). Joint angle data were sampled at 100 Hz, and recorded in sync with EEG data using our customized C++ program. Three wireless inertial motion sensors (OPAL, APDM Inc., Portland, OR) were mounted on subject's head, left heel, and right heel. Each sensor included accelerometer, gyroscope, and magnetometer sampled at 128Hz. The two sensors on the feet provided timing for the gait cycles. OPAL data was synchronized with EEG and goniometer data. Figure 2 shows raster plot of these signals.

2.3.Signal Pre-processing

All processing was carried out in custom C++ software in real-time. A robust adaptive filter was applied to allow real-time filtering of eye-blink and eye-motion artifacts using data recorded from EOG channels (Kilicarslan et al., 2016). Peripheral EEG channels were removed as they are most susceptible to artifacts from head movements, and facial/cranial muscle activity. EEG in the delta band (0.1 – 3 Hz) was used for neural decoding of treadmill walking; thus, the EEG features correspond to time-domain amplitude modulated (AM) potentials in the delta band. The 0 – 3 Hz band was known to cover most power in joint angle signals (Antonsson and Mann, 1985, Luu et al., 2014, Luu et al., 2015). Moreover, in (Nathan and Contreras-Vidal, 2016), we have shown that motion artifacts are negligible at the gait speeds used in our study. In that study, the authors conducted intensive analysis of potential motion artifacts in scalp EEG recording during treadmill walking and

suggested that subjects' motion did not significantly affect their EEG at the gait speeds reported in this research.

2.4.Unscented Kalman Filter Decoder

Linear decoders such as Wiener filters and Kalman filters are most commonly used in BCI applications (Wu et al., 2006). However, these models cannot handle a non-linear relationship between neural activities and limb movements. Recently, Li *et al.* showed that the unscented Kalman filter outperformed the Kalman filter and the Wiener filter in both offline and real-time BCI operation (Li et al., 2009). In this study, UKF was used as decoder and defined by four parameter matrices F, B, Q, and R; the UKF algorithm was based on (Li et al., 2009). The state variable at time t was defined as:

$$x_t=[\theta_{\mathrm{rh}},\theta_{\mathrm{lh}},\theta_{\mathrm{rk}},\theta_{\mathrm{lk}},\theta_{\mathrm{ra}},\theta_{\mathrm{la}}]^T$$

where θ denotes the joint angle; h,k, and a represent hip, knee, and ankle, respectively.

UKF started with a prediction step which estimated the current state:

$$x_{t'}=\mathrm{F}x_{t-1}$$

$$P_{t'}=\mathrm{F}P_{t-1}F^T+Q$$

where $x_{t'}$ and $P_{t'}$ are the predicted state and its covariance; x_{t-1} and P_{t-1} are the previous state and its covariance.

The prediction step was followed by the updating step which used observation data (EEG) to correct the predicted values. In this step, an unscented transformation was used to obtain sigma points as:

$$X_0=x_{t'}$$

$$X=x_{t'}+\left(\sqrt{(d+k)P_{t'}}\right)_i, i=1..d$$

$$X=x_{t'}-\left(\sqrt{(d+k)P_{t'}}\right)_{i-d}, i=d+1..2d$$

where d is the size of x_t, $d=6$; k determines the spread of the sigma points, $k=1$ for normal distribution.

Each sigma point X_i was then augmented and evaluated in an observation function as:

$$X_{\text{aug}}=[\theta_{\text{rh}},\theta_{\text{lh}},\sqrt{\theta_{\text{rh}}^2+\theta_{\text{lh}}^2},\theta_{\text{rk}},\theta_{\text{lk}},\sqrt{\theta_{\text{rk}}^2+\theta_{\text{lk}}^2},\theta_{\text{ra}},\theta_{\text{la}},\sqrt{\theta_{\text{ra}}^2+\theta_{\text{la}}^2}]^T$$

$$Z_i=\text{BX}_{\text{aug}},i=0..2d$$

The predicted neural signals and its covariance were calculated as:

$$z_t=\sum_{i=0..2d} w_i Z_i$$

$$P_{\text{zz},t}=w_0(Z_0-z_t)(Z_0-z_t)^T+\sum_{i=1..2d} w_i(Z_i-Z_0)(Z_i-Z_0)^T+R$$

The weights w_i were defined as:

$$w_0=\frac{k}{d+k}$$

$$w_i=\frac{1}{2(d+k)},i=1..2d$$

The Gaussian partial pivoting method was used to solve the following equation for Kalman gain.

$$P_{\text{zz},t}K=P_{\text{xz},t}$$

where $P_{xz,t}$ is the state-observation cross covariance:

$$P_{\text{xz},t}=w_0(X_0-x_{t'})(Z_0-z_t)^T+\sum_{i=1..2d} w_i(X_i-X_0)(Z_i-Z_0)^T$$

The estimated state was corrected and the state covariance was also updated:

$$x_t=x_{t'}+K_t(y_t-z_t)$$

$$P_t=P_{t'}+K_tP_{\text{zz},t}K_t^T$$

2.5.Online Updates of UKF Parameters

BCI decoders are typically trained offline by fitting neural signals against kinematic data. During closed-loop BCI, the subjects can alter their neural activity and affect the accuracy of the trained decoder which does not account for the difference in neural activity. Recently, Orsborn *et al.* showed that closed-loop decoder adaptation (CLDA) where decoder parameters are updated during closed-loop BCI operation can yield performance improvements (Orsborn et al., 2011). To apply CLDA for the UKF decoder in this study, the pre-processed EEG and lower limb joint angles were first streamed to a buffer which stores 1 min of collected data (6000 samples). After data in the buffer were collected, the UKF's parameters were updated using parameter fitting method introduced in (Li et al., 2009). The pre-processing steps, CLDA updates and real-time decoding of the EEG based BCI-VR system are depicted in Figure 3.

2.6.Assessment of real-time decoder's performance

To quantify the level of accuracy for real-time decoding of lower limb joint angles, the Pearson's r-values between measured and predicted joint angles were computed for the *gonio-control* and *EEG-control* phases.

EEG signals were first analyzed by mean, standard deviation (STD), and signal to noise ratio (SNR). These values were calculated from sliding windows with window size of 30s and step size of 1s. EEG artifacts from stereotypical (e.g., eye blinks) and non-stereotypical (e.g., movement, muscle bursts) sources were removed using Artifact Subspace Reconstruction (ASR) method which is available as a plug-in for EEGLAB software (Delorme and Makeig, 2004). The outputs from ASR method (EEG_{ASR}) and EEG raw data were used to estimate EEG noise and compute SNR values. The results were grouped based on EEG sensor locations: peripheral (PERI), Frontal (F), Central (C), and Posterior (P) electrodes.

$$\mathrm{SNR}_W = 10\log 10 \frac{\sum_i^N (\mathrm{EEG}^i_{\mathrm{raw}})^2}{\sum_i^N (\mathrm{EEG}^i_{\mathrm{raw}} - \mathrm{EEG}^i_{\mathrm{ASR}})^2}$$

where SNR_w is signal to noise ratio of EEG data in window w^{th}; i = 1..N is EEG samples in one window.

2.7.Assessment of gait adaptation to visual kinematic perturbations

Gait symmetry provides information about the control of human walking. Analyzing gait symmetry is clinically significant (Patterson et al.). In general, there are two components that determine a symmetry metric: an equation to calculate gait symmetry and the spatial-temporal gait parameters used in the equation (e.g., stride length, step length, range of motion, cadence, stance time, swing time, etc.) (Patterson et al., 2010). The symmetry ratio (SR) and range of motion (ROM) of the avatar's lower limbs were used to calculate gait symmetry and thus, the quality of EEG-based avatar control.

$$\mathrm{SR}_g = \frac{\mathrm{ROM}_{r,g}}{\mathrm{ROM}_{l,g}}$$

where *g* represents hip, knee or ankle joints; *r* and *l* are right and left leg, respectively.

3.Results

3.1.Gait adaptation to visual kinematic perturbation

We observed changes in errors between lower limb joint angles of the subjects and the walking avatar during visual kinematic perturbation. Figure 4 depicts the errors during exposure and post-exposure phases in 8 days for knee joint angles. The errors were standardized (z-score) with pre-exposure phase as baseline. In pre-exposure phase, the walking avatar was controlled by predicted lower limb joint angles (hip, knee, and ankle) from real-time decoder; however, in exposure, the introduction of kinematic perturbations (predicted joint angles were multiplied by 0.7) resulted in changes in the errors compared with the pre-exposure phase. After removal of the visual kinematic perturbation during the post-exposure phase, joint angles errors changed in the opposite direction as during exposure (i.e., after-effect). Nevertheless, the errors between subjects' and the walking avatar's joint angles during exposure and post-exposure decreased in 8 days of training.

3.2.Effects of visual kinematic perturbation on movement control and closed-loop BCI control

Figure 5 illustrates the effects of visual kinematic perturbation on both subject's lower limb movement control and closed-loop BCI control of the walking avatar. Range of motion ratios between 4 right and left joint angles were used as a gait symmetry index. ROM ratios were first standardized (z-5 score) against *gonio-control* phase; the differences between ROM ratios in post- and pre-exposure phases 6 were analyzed using pairwise *t*-test. Results in Figure 5 shows that the introduction of visual kinematic 7 perturbation significantly affected both subject's movement control and avatar's BCI control. In general, 8 the differences in ROM ratios of subjects SK03 and SK04 in Day 8 decreased compare to Day 1. The changes of subjects' and avatar's ROM ratios are different under visual kinematic perturbation and these changes varied across subjects.

Figure 6 shows the numbers of sessions with ROM ratios significantly affected by visual kinematic perturbation. As can be seen, the introduction of visual kinematic perturbation affected the BCI control of the walking avatar more than the subjects' movement control for subjects SK03 and SK04. Nevertheless, the opposite results were found for subjects SK01 and SK02.

3.3.Real-time decoding accuracies improved within 8 days of training

The improvement of decoding lower limb joint angles (hip, knee, and ankle) from scalp EEG signals can be found as in Figure 7, Figure 8 and Figure 11. Figure 7A shows examples of the measured and reconstructed lower limb joint angles (hip, knee, and ankle) and heel positions (calculated from lower limb joint angles) for subject SK04 on Day 1 and Day 8. As

can be seen, the reconstructed kinematics on Day 8 are closer and more in-phase with the actual values compared to the reconstructed values on Day 1. The quality of the reconstructions of gait trajectories in 3D space on Day 1 and Day 8 is also illustrated in Figure 7B. Polar plot in Figure 8 shows that r-values on Day 8 are closer to the circle (r = 1) compare to these values on Day 1. In Figure 11, low decoding accuracies are depicted in blue, and they are concentrated on Day 1. Decoders become better within 8 days and the high decoding accuracies, shown in brown, are concentrated on Day 8. Decoding accuracies of lower limb joint angles for 4 subjects on Day 1 and Day 8 were also calculated and reported in Table 1. Decoding accuracies of lower limb joint angles on Day 8 are higher than decoding accuracies on Day 1, except for SK01's hip joint.

3.4.Real-time decoding accuracies varied across subjects

The accuracies of decoding lower limb joint angles (hip, knee, and ankle) from scalp EEG signals for the 4 subjects across 8 days are illustrated in polar plot in Figure 8. The shaded areas indicate one standard deviation of r-values. In the polar plot, r = 0 at the center of the circle and r = 1 on the perimeter of the circle. Among the subjects, SK04 has decoders with the highest r-values.

Statistical analysis between subjects was performed using pairwise *t*-test with Tukey-Kramer adjustment for multiple comparison and the results are shown in Figure 9. Pearson's r-values for subject SK04 are significantly different from the others ($P < 0.001$). R-values for SK03 and SK01 are also significantly different ($P < 0.05$). One-way ANOVA was also performed to confirm that r-values differed across subjects ($P < 0.001$).

3.5.Effects of EEG signals quality on real-time decoding accuracies

The analysis of EEG signals (Mean, standard deviation (STD), and signal to noise ratio (SNR)), and Pearson's r-values between actual and predicted lower limb joint angles (hip, knee, and ankle) for subject SK04 across 8 days are shown in Figure 10. Sliding windows (window size of 5s and step size of 0.5s) were used to analyze EEG and kinematic data. EEG channels are grouped into 4 regions: Pre-Frontal (PF), Frontal (F), Central (C) and Parietal (P). In general, the STD of EEG signals decreased and the SNR of EEG signals increased across the 8 days. The stability of EEG signals also improved across days. Compared with EEG signals in central and parietal areas, EEG signals in pre-frontal and frontal areas have higher STD and lower SNR values. Figure 10 shows that Pearson's r-values for hip, knee, and ankle joint increased and became more stable within 8 days of training. Moreover, decoding accuracies varied across lower limb joints (hip, knee, and ankle). For example, r-values between actual and predicted angles increased from 0.31 ± 3.31 (Day 1) to 0.72 ± 0.12 (Day 8) for the hip, 0.41 ± 0.26 to 0.81 ± 0.08 for the knee, and from 0.16 ± 0.25 to 0.45 ± 0.20 for the ankle joint.

It was expected that the decoding accuracy (r-values) would improve with low STD and high SNR values of EEG signals. Figure 11 illustrates the effects of STD and SNR values of EEG signals on decoding accuracy. High decoding accuracies ($r > 0.5$) are depicted in brown color and they concentrate at the top left of the plot. This area has relatively low STD (< 11 μV) and high SNR values (> −8 dB). On the other hand, low decoding accuracies ($r < 0.3$)

are shown in blue and they concentrate at the bottom right of the plot (STD > 20 μV and SNR < −12 dB).

4.Discussion

In this study, a real-time neural decoder was designed to translate neural activity acquired via scalp EEG into lower limb movements in human walking. The predicted lower limb joint angles (hip, knee, and ankle) were used to control a walking avatar in a virtual environment. Visual kinematic perturbations of gait patterns were also introduced to investigate cortical adaptations during gait adaptation using a closed-loop EEG-based BCI.

Historically, Brain-Computer Interface (BCI) research has been primarily conducted for communication or for upper arm pointing movements (e.g., center-out paradigm where the number of targets, accuracy and the speed of acquisition are important), and more recently for use to control assistive devices or neuroprostheses. One metric used in BCIs for communication and center-out hand movements has been the 'bit rate', which can be computed from task parameters (e.g., number of symbols to communicate in the case of communicative BCI spellers and number of targets, target size and movement time in the case of BCIs used for center-out movements). The bit-rate for these systems (invasive or not) used by people with disabilities remains unfortunately low (< 2 bits/sec), except for recent demonstrations in monkey dorsal premotor cortex, which has reached up to 6.5 bits/sec, or approximately 15 words per minute, with 96 implanted electrodes (Santhanam et al., 2006). A walking gait cycle could be divided into two main phases: stance phase which comprises approximately 62% of the gait cycle, and swing phases which comprises 38% of the cycle. The information content for discrete classification of stand and swing phases could be computed as: 0.6 * (−log(0.6)) + 0.4 * (−log(0.4)) = 0.67 bits; and the information rate for walking on treadmill at gait speed of 1 mph is 0.67 / 1.65 = 0.41 bits/sec, where 1.65 (s) is the average of gait cycle time in this study. Note that the neural decoder in this study was not designed for gait cycle classification; the outputs from the decoder were lower limb joint angles instead. The use of 'information rate' as a metric to assess BCIs for the control of prosthetic limbs and exoskeletons may not be appropriate because suitable metrics should measure functional outcomes and usability of those technologies, e.g., can the amputee complete a successful grasp? Can the stroke patients regain gait symmetry? For a discussion of metrics, see (Contreras-Vidal, 2014).

Our EEG-based Kalman decoders were designed to close the loop in a BCI with update rates that are faster than the rate of the actual or predicted movements. First, the closed-loop neural interfaces are updated often (~ 10 msec) so that real-time control can be achieved; second, most gait movements, particularly in rehabilitation contexts, have a very low bandwidth (usually < 3 Hz), which is known to cover most power in joint angle signals (Antonsson and Mann, 1985, Luu et al., 2014). Moreover, we have shown that motion artifacts are negligible in these frequencies (Nathan and Contreras-Vidal, 2016), and have demonstrated that Wiener and Kalman filters can be used for decoding continuous linear kinematics from the fluctuations of the amplitude (i.e., amplitude modulation) of slow cortical potentials in the delta band EEG that compares well to invasive BCI approaches (Presacco et al., 2011). Other groups have also shown that gait information is contained in

low frequencies of EEG; for example, Gwin et al. showed that meaningful changes in EEG during walking or running occur at low frequency (< 10 Hz) (Gwin et al., 2010). In this manuscript, we show that our EEG Kalman decoders operating in the fluctuations in the amplitude of slow cortical potentials in the delta band can be used to close the loop in a BCI with update rates that are faster than the rate of the actual or predicted movements. The bandwidth of these time-domain delta band features are commensurable with the bandwidth of the gait movements performed by the subjects in this and other gait studies.

We observed that the subjects were able to adapt the avatar's gait patterns controlled via the closed-loop EEG-based BCI. The improvement of real-time decoding accuracies in 8 days of training suggests that with practice, subjects gained more control of the walking avatar by using their brain signals. This finding supports the view that the visuomotor adaptation can be triggered directly from brain activity and thus the proposed system can also be used as a platform to examine cortical plasticity in the human brain. We found that decoding accuracies (or r-values) varied with the mean, STD and SNR scores of the EEG signals, suggesting that signal stability within and across days may be influenced by global internal states of the subjects such as attention, motivation and fatigue. These global states should be quantified in future studies.

Asymmetric walking gait patterns are commonly found in patients post-stroke. Study of walking adaptation to a split-belt perturbation, which creates early asymmetric walking, demonstrated that with practice, subjects can improve phasing and reduce gait asymmetry (Malone et al., 2012). Moreover, the understanding of gait adaptation may suggest appropriate interventions for gait rehabilitation. In this study, a closed-loop BCI was used to investigate if changes in brain activity contribute to gait adaptation during virtual kinematic perturbation of a walking avatar in a virtual environment. The results show that the visual kinematic perturbation affected both the movement control of subjects' lower limb and BCI control of the walking avatar. Interestingly, walking gait patterns of the subjects and the walking avatar improved in phasing and similarity with practice suggesting the BCI-avatar system triggered cortical plasticity. The results also showed that the adaptation of BCI control and movement control differed between subjects when visual kinematic perturbation was introduced. For example, more BCI control of the walking avatar was found for SK03 and SK04 while more movement control was found for SK01 and SK02 (Figure 6). Interestingly, SK03 and SK04 have better decoding accuracies compare to SK01 and SK02 (Figure 9). This suggests that subjects might focus more on BCI control of the walking avatar under visual kinematic perturbation if a good real-time neural decoder was provided.

Previous studies demonstrated that BCI applications and VR-based neurorehabilitation systems enhance active participation and contribute to significantly better motor functional outcomes in motor rehabilitation (Pichiorri et al., 2015, Morone et al., 2015, Saleh et al., 2011, Cameirão et al., 2012, da Silva Cameirão et al., 2011, Brütsch et al., 2011). The integration of BCI and VR technologies is expected to be very promising (Lotte et al., 2013). Pfurtscheller et al. introduced a BCI system using motor imagery (MI) to navigate in a virtual environment (Leeb et al., 2007, Friedman et al., 2007). The combination of BCI and VR could be beneficial for rehabilitation purposes. However, the number of studies of noninvasive BCI-VR in the context of neurorehabilitation is limited. In this study, we

observed that the subjects were able to control a walking avatar via a closed-loop EEG-based BCI-VR system. In addition, the improvement of real-time decoding accuracies in 8 days of training illustrates that with practice, subjects gained more control of the walking avatar by using their brain signals in spite of the conflicting sensory and motor signals. We note that subjects were instructed to keep their gait pattern consistent and control the walking avatar only by using their brain signals and that the changes of their own actual walking for asymmetry compensation didn't contribute to the real-time decoding performance as the decoding accuracies (r-values) were calculated from neural decoder outputs and measured joint angles from the right leg (i.e., the avatar's right leg was driven by brain signals during *eeg-control* phase and affected by visual kinematic perturbation). The results suggest that the proposed EEG-based BCI-VR could be feasible in visuomotor learning and beneficial to the field of neurorehabilitation.

Observational therapy in stroke rehabilitation has been found to be beneficial (Celnik et al., 2008, Ertelt et al., 2007, Franceschini et al., 2012). In typical observational therapy, persons with stroke observe a video clip or other people demonstrating a movement before they try it themselves. Reports suggest that patients undergoing observational therapy show significant improvement in functional assessment, including fMRI, before and after the treatment (Ertelt et al., 2007). Inspired by this fact, we propose to enhance patient involvement by allowing them to use their neural activity to control an avatar instead of passively watching movement. In this regard, we also examined how visual disruption affected the *gonio-control* phase. A clear adapting phase and learning curve can be seen during the perturbation (Figure 4), showing that the subjects were actively learning the new motor coordination skills. We hypothesize that the proposed EEG-based BCI-VR could be feasible and beneficial to observational therapy in stroke rehabilitation. Moreover, the proposed EEG-based neural decoder could be integrated with robotic assisted devices or robotic orthosis for lower limbs to facilitate advanced neurorehabilitation interventions.

Neural decoders play a central role in BCI applications. Although results from decoder accuracies in this study are promising, some limitations need to be considered in future research. First, the decoding accuracies for ankle joint angles are significantly lower than those for hip and knee joint angles. Second, even though the proposed real-time neural decoder provided good accuracy in terms of Pearson's r-values (up to 0.81 ± 0.08 in 50 mins session) and phasing between measured and predicted lower limb joint angles, the errors between the measured and predicted values need to be further reduced. The signal to noise ratio between actual and predicted joint angles will be considered as an assessment parameter when improving the neural decoder. Finally, the neural decoder in this study is limited to only inferring lower limb joint angles from EEG signals for a walking gait pattern at 1mph. Further analysis to enhance the neural decoder for a wider range of gait speeds is required.

A robust adaptive filter was applied to allow real-time filtering of eye-blink and eye-motion artifacts using data recorded from EOG channels for subjects SK03 and SK04 (this filter was not available when subjects SK01 and SK02 were tested). This filter significantly increased decoding accuracy of user intentions using EEG to control a lower-body exoskeleton, as it was shown in (Kilicarslan et al., 2016). A previous study showed that quality of EEG signals

(i.e., signal to noise ratio, standard deviation) affect decoding accuracies of treadmill walking (Luu et al., 2015), which was the case in this research. Therefore, the implementation of real-time filtering of eye-blink and eye-motion artifacts was expected to yield higher decoding accuracy for SK03 and SK04 than for SK01 and SK02. Moreover, the quality of EEG signals recorded from SK03 and SK04 was significantly different. Pairwise *t*-test was applied to compare signal to noise ratios and standard deviation of EEG signals for SK03 and SK04. The results showed that SK04 had higher SNR (SK03: −11.64 ± 3.45; SK04: −8.91 ± 2.03; $P < 0.001$) and lower STD values (SK03: 18.96 ± 3.44; SK04: 12.78 ± 2.03; $P < 0.001$). The implementation of real-time artifacts removal and the high quality of EEG signals might explain why SK04's performances were significantly superior to the other three subjects. However, future works on analysis of how robust adaptive filter affects neural decoding accuracies of treadmill walking are required for better understanding. Studies have shown the central nervous system's capacity to adapt its structural organization after the development of a brain lesion (Masiero et al., 2014). Such brain lesions can also be simulated in our settings by deliberately removing certain EEG channels that are input to the decoder. With such a change, decoder performance is expected to drop and trigger neural adaptation to restore function. Study of adaptation to virtual cortical lesions within the proposed EEG-based BCI-VR system will be considered in future directions.

Examining the changes in the representation of gait in cortical networks during virtual kinematics perturbation is one of main objectives of this research. Future studies will consider analyzing power of EEG signal in different bands and performing EEG source localization to understand the neural sources of cortical plasticity during closed-loop BCI learning and virtual kinematics perturbations.

Acknowledgments

This research was supported by award R01NS075889 from the National Institute of Neurological Disorders And Stroke (NINDS). The content is solely the responsibility of the authors and does not necessarily represent the official views of the NINDS or the National Institutes of Health (NIH). The authors would like to thank Kevin Nathan and Jeffrey Gorges for their assistance with the data collection.

References

Antonsson EK, Mann RW. The frequency content of gait. Journal of Biomechanics. 1985; 18:39–47. [PubMed: 3980487]

Bohil CJ, Alicea B, Biocca FA. Virtual reality in neuroscience research and therapy. Nat Rev Neurosci. 2011; 12:752–762. [PubMed: 22048061]

Brütsch K, Koenig A, Zimmerli L, Mérillat-Koeneke S, Riener R, Jäncke L, Van Hedel HJA, Meyer-Heim A. Virtual reality for enhancement of robot-assisted gait training in children with central gait disorders. J Rehabil Med. 2011; 43:493–499. [PubMed: 21491072]

Brutsch K, Schuler T, Koenig A, Zimmerli L, Koeneke SM, Lunenburger L, Riener R, Jancke L, Meyer-Heim A. Influence of virtual reality soccer game on walking performance in robotic assisted gait training for children. J Neuroeng Rehabil. 2010; 7:15. [PubMed: 20412572]

Bulea TC, Prasad S, Kilicarslan A, Contreras-Vidal JL. Sitting and Standing Intention Can be Decoded from Scalp EEG Recorded Prior to Movement Execution. Frontiers in Neuroscience. 2014; 8

Cameirão MS, Badia SBI, Duarte E, Frisoli A, Verschure PFMJ. The combined impact of virtual reality neurorehabilitation and its interfaces on upper extremity functional recovery in patients with chronic stroke. Stroke. 2012; 43:2720–2728. [PubMed: 22871683]

Celnik P, Webster B, Glasser DM, Cohen LG. Effects of action observation on physical training after stroke. Stroke. 2008; 39:1814–20. [PubMed: 18403746]

Chéron G, Duvinage M, De Saedeleer C, Castermans T, Bengoetxea A, Petieau M, Seetharaman K, Hoellinger T, Dan B, Dutoit T. From spinal central pattern generators to cortical network: integrated BCI for walking rehabilitation. Neural plasticity. 2012; 2012

Contreras-Vidal JL. Identifying engineering, clinical and patient's metrics for evaluating and quantifying performance of brain-machine interface (BMI) systems. Systems, Man and Cybernetics (SMC), 2014 IEEE International Conference on. Oct 5–8.2014 2014:1489–1492.

Da Silva Cameirão M, Bermudez I Badia S, Duarte E, Verschure PFMJ. Virtual reality based rehabilitation speeds up functional recovery of the upper extremities after stroke: a randomized controlled pilot study in the acute phase of stroke using the rehabilitation gaming system. Restorative neurology and neuroscience. 2011; 29:287–298. [PubMed: 21697589]

Delorme A, Makeig S. EEGLAB: an open source toolbox for analysis of single-trial EEG dynamics including independent component analysis. Journal of neuroscience methods. 2004; 134:9–21. [PubMed: 15102499]

Ertelt D, Small S, Solodkin A, Dettmers C, Mcnamara A, Binkofski F, Buccino G. Action observation has a positive impact on rehabilitation of motor deficits after stroke. Neuroimage. 2007; 36:T164–T173. [PubMed: 17499164]

Fitzsimmons NA, Lebedev MA, Peikon ID, Nicolelis MA. Extracting kinematic parameters for monkey bipedal walking from cortical neuronal ensemble activity. Frontiers in integrative neuroscience. 2009; 3

Franceschini M, Ceravolo MG, Agosti M, Cavallini P, Bonassi S, Dall'armi V, Massucci M, Schifini F, Sale P. Clinical relevance of action observation in upper-limb stroke rehabilitation a possible role in recovery of functional dexterity. A randomized clinical trial. Neurorehabilitation and Neural Repair. 2012; 26:456–462. [PubMed: 22235059]

Friedman D, Leeb R, Guger C, Steed A, Pfurtscheller G, Slater M. Navigating virtual reality by thought: What is it like? Presence: Teleoperators and Virtual Environments. 2007; 16:100–110.

Gwin JT, Gramann K, Makeig S, Ferris DP. Removal of movement artifact from high-density EEG recorded during walking and running. Journal of neurophysiology. 2010; 103:3526–3534. [PubMed: 20410364]

Hashimoto Y, Ushiba J, Kimura A, Liu M, Tomita Y. Change in brain activity through virtual reality-based brain-machine communication in a chronic tetraplegic subject with muscular dystrophy. BMC Neurosci. 2010; 11:117. [PubMed: 20846418]

Holden MK. Virtual environments for motor rehabilitation: review. Cyberpsychol Behav. 2005; 8:187–211. discussion 212-9. [PubMed: 15971970]

Hsu A-L, Tang P-F, Jan M-H. Analysis of impairments influencing gait velocity and asymmetry of hemiplegic patients after mild to moderate stroke. Archives of physical medicine and rehabilitation. 2003; 84:1185–1193. [PubMed: 12917858]

Jaffe DL, Brown DA, Pierson-Carey CD, Buckley EL, Lew HL. Stepping over obstacles to improve walking in individuals with poststroke hemiplegia. J Rehabil Res Dev. 2004; 41:283–92. [PubMed: 15543446]

Kilicarslan A, Grossman RG, Contreras-Vidal JL. A robust adaptive denoising framework for real-time artifact removal in scalp EEG measurements. J Neural Eng. 2016; 13:026013. [PubMed: 26863159]

Kilicarslan, A., Prasad, S., Grossman, RG., Contreras-Vidal, JL. Engineering in Medicine and Biology Society (EMBC), 2013 35th Annual International Conference of the IEEE. IEEE; 2013. High accuracy decoding of user intentions using EEG to control a lower-body exoskeleton; p. 5606-5609.

King CE, Wang PT, Chui LA, Do AH, Nenadic Z. Operation of a brain-computer interface walking simulator for individuals with spinal cord injury. J Neuroeng Rehabil. 2013; 10:77. [PubMed: 23866985]

Lamontagne A, Fung J. Faster is better implications for speed-intensive gait training after stroke. Stroke. 2004; 35:2543–2548. [PubMed: 15472095]

Leeb R, Lee F, Keinrath C, Scherer R, Bischof H, Pfurtscheller G. Brain-computer communication: motivation, aim, and impact of exploring a virtual apartment. IEEE Trans Neural Syst Rehabil Eng. 2007; 15:473–482. [PubMed: 18198704]

Li Z, O'doherty JE, Hanson TL, Lebedev MA, Henriquez CS, Nicolelis MA. Unscented Kalman filter for brain-machine interfaces. PloS one. 2009; 4:e6243. [PubMed: 19603074]

Llorens R, Gil-Gomez JA, Alcaniz M, Colomer C, Noe E. Improvement in balance using a virtual reality-based stepping exercise: a randomized controlled trial involving individuals with chronic stroke. Clin Rehabil. 2015; 29:261–8. [PubMed: 25056999]

Lotte, F., Faller, J., Guger, C., Renard, Y., Pfurtscheller, G., Lécuyer, A., Leeb, R. Combining BCI with Virtual Reality: Towards New Applications and Improved BCI. In: Allison, BZ.Dunne, S.Leeb, R.Del, R.Millán, J., Nijholt, A., editors. Biological and Medical Physics, Biomedical Engineering. Springer Berlin Heidelberg; 2013.

Luu, TP., He, Y., Brown, S., Nakagome, S., Contreras-Vidal, JL. A closed-loop brain computer interface to a virtual reality avatar: Gait adaptation to visual kinematic perturbations; 2015 International Conference on Virtual Rehabilitation (ICVR); 2015. p. 30-37.

Luu TP, Low KH, Qu X, Lim HB, Hoon KH. An individual-specific gait pattern prediction model based on generalized regression neural networks. Gait & Posture. 2014; 39:443–448. [PubMed: 24071020]

Malone LA, Bastian AJ, Torres-Oviedo G. How does the motor system correct for errors in time and space during locomotor adaptation? Journal of neurophysiology. 2012; 108:672–683. [PubMed: 22514294]

Masiero S, Poli P, Rosati G, Zanotto D, Iosa M, Paolucci S, Morone G. The value of robotic systems in stroke rehabilitation. Expert review of medical devices. 2014; 11:187–198. [PubMed: 24479445]

Morone G, Pisotta I, Pichiorri F, Kleih S, Paolucci S, Molinari M, Cincotti F, Kübler A, Mattia D. Proof of principle of a brain-computer interface approach to support poststroke arm rehabilitation in hospitalized patients: design, acceptability, and usability. Archives of physical medicine and rehabilitation. 2015; 96:S71–S78. [PubMed: 25721550]

Nathan K, Contreras-Vidal JL. Negligible motion artifacts in scalp electroencephalography (EEG) during treadmill walking. Frontiers in Human Neuroscience. 2016; 9

Orsborn AL, Dangi S, Moorman HG, Carmena JM. Exploring time-scales of closed-loop decoder adaptation in brain-machine interfaces. Conf Proc IEEE Eng Med Biol Soc. 2011; 2011:5436–9. [PubMed: 22255567]

Patterson KK, Gage WH, Brooks D, Black SE, Mcilroy WE. Evaluation of gait symmetry after stroke: a comparison of current methods and recommendations for standardization. Gait Posture. 2010; 31:241–6. [PubMed: 19932621]

Patterson KK, Parafianowicz I, Danells CJ, Closson V, Verrier MC, Staines WR, Black SE, Mcilroy WE. Gait Asymmetry in Community-Ambulating Stroke Survivors. Archives of Physical Medicine and Rehabilitation. 89:304–310. [PubMed: 18226655]

Pichiorri F, Morone G, Petti M, Toppi J, Pisotta I, Molinari M, Paolucci S, Inghilleri M, Astolfi L, Cincotti F, Mattia D. Brain-computer interface boosts motor imagery practice during stroke recovery. Annals of neurology. 2015; 77:851–865. [PubMed: 25712802]

Presacco A, Goodman R, Forrester L, Contreras-Vidal JL. Neural decoding of treadmill walking from noninvasive electroencephalographic signals. Journal of neurophysiology. 2011; 106:1875–1887. [PubMed: 21768121]

Reisman DS, Wityk R, Silver K, Bastian AJ. Split-belt treadmill adaptation transfers to overground walking in persons poststroke. Neurorehabilitation and neural repair. 2009; 23:735–744. [PubMed: 19307434]

Rizzo A, Kim GJ. A SWOT analysis of the field of virtual reality rehabilitation and therapy. Presence: Teleoper. Virtual Environ. 2005; 14:119–146.

Saleh S, Bagce H, Qiu Q, Fluet G, Merians A, Adamovich S, Tunik E. Mechanisms of neural reorganization in chronic stroke subjects after virtual reality training. Conf Proc IEEE Eng Med Biol Soc. 2011; 2011:8118–8121. [PubMed: 22256226]

Santhanam G, Ryu SI, Yu BM, Afshar A, Shenoy KV. A high-performance brain–computer interface. Nature. 2006; 442:195–198. [PubMed: 16838020]

Venkatakrishnan A, Francisco GE, Contreras-Vidal JL. Applications of Brain–Machine Interface Systems in Stroke Recovery and Rehabilitation. Current Physical Medicine and Rehabilitation Reports. 2014; 2:93–105. [PubMed: 25110624]

Wang PT, King CE, Chui LA, Do AH, Nenadic Z. Self-paced brain–computer interface control of ambulation in a virtual reality environment. Journal of neural engineering. 2012; 9:056016. [PubMed: 23010771]

Wu W, Gao Y, Bienenstock E, Donoghue JP, Black MJ. Bayesian Population Decoding of Motor Cortical Activity Using a Kalman Filter. Neural Comput. 2006; 18:80–118. [PubMed: 16354382]

Yang Y-R, Tsai M-P, Chuang T-Y, Sung W-H, Wang R-Y. Virtual reality-based training improves community ambulation in individuals with stroke: a randomized controlled trial. Gait & posture. 2008; 28:201–206. [PubMed: 18358724]

You SH, Jang SH, Kim YH, Hallett M, Ahn SH, Kwon YH, Kim JH, Lee MY. Virtual reality-induced cortical reorganization and associated locomotor recovery in chronic stroke: an experimenter-blind randomized study. Stroke. 2005; 36:1166–71. [PubMed: 15890990]

Yuan H, Perdoni C, He B. Relationship between speed and EEG activity during imagined and executed hand movements. Journal of neural engineering. 2010; 7:026001.

Phases	Rest	*Gonio-control*	*EEG-control*			Rest
			Pre-	Exposure	Post-	
Time (mins)	2	15	8	15	8	2
Decoder status	-	CLDA updating		Fixed		-

Figure 1.

The experimental procedure for each day. Each session lasted approximately 50 mins. Subjects were instructed to have 2 mins of standing still at the beginning and at the end of experiment while looking at the avatar and try to minimize eye blinks. In the *gonio-control* phase (15 mins), the avatar was driven by goniometer signals. Decoder parameters were updated every 1 min and fixed by the end of this phase by using closed-loop decoder adaptation (CLDA). In the *EEG-control* phase, the avatar's right leg was driven by decoder outputs. During exposure phase, decoder outputs were linearly scaled down by the perturbation gain, 0.7.

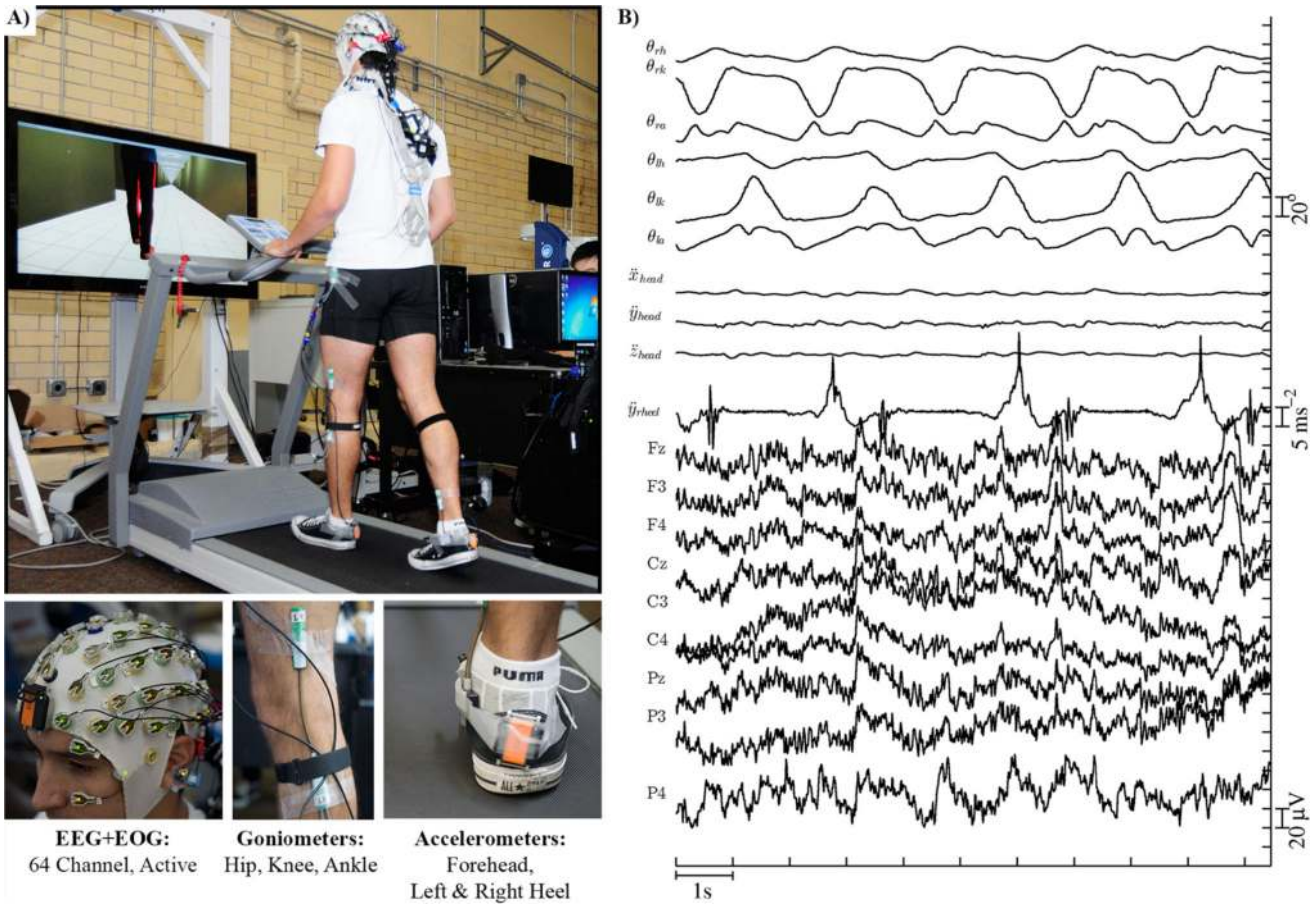

Figure 2.

A) Experimental setup in this study. Each subject was instructed to walk on a treadmill at 1mph and think about controlling an avatar to walk normally while looking at the avatar displayed in VE in front of them. Recorded data included electroencephalography (EEG) and electrooculogram (EOG), lower limb joint angles of both left and right leg, and accelerations of head, left and right heel. B) Example of raw data in 10 seconds.

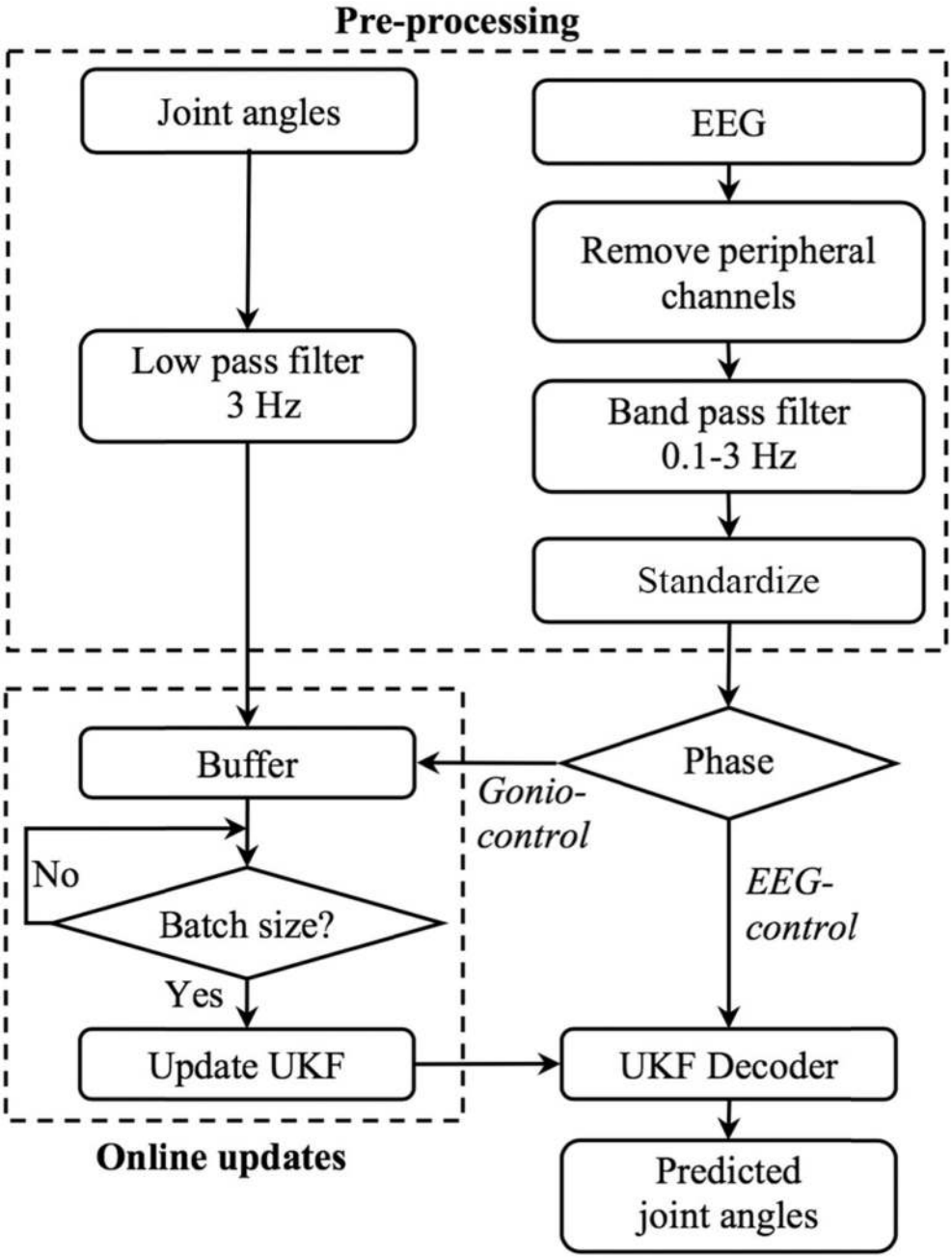

Figure 3.

Flow chart of kinematics and EEG signal pre-processing, online updates for unscented Kalman filter parameters and avatar control in this study.

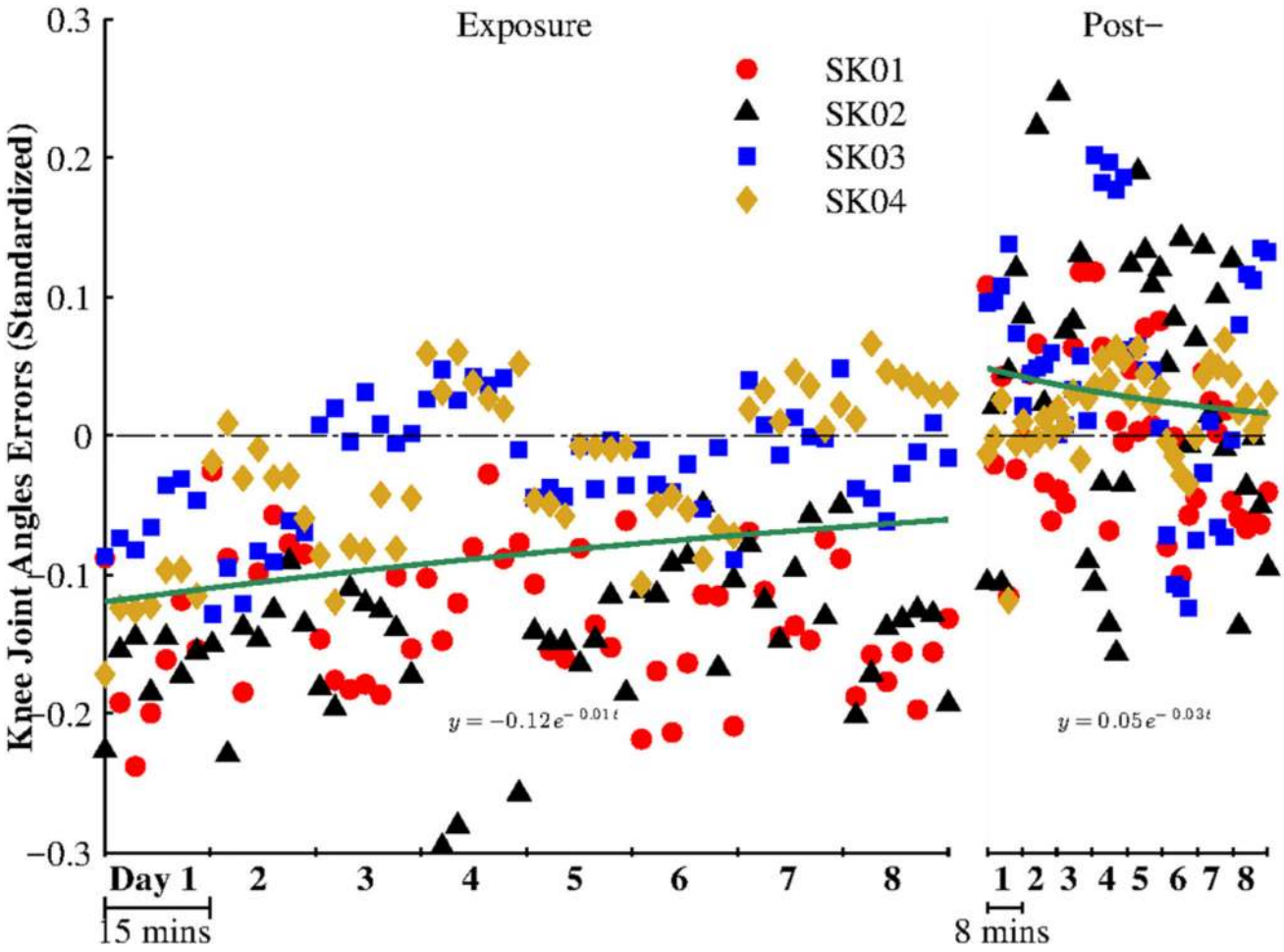

Figure 4.

Errors between right knee joint angles of the subjects and the walking avatar during visual kinematic perturbation. The errors were standardized (baseline: *pre-exposure* phase). Solid lines are exponential fit for all data points.

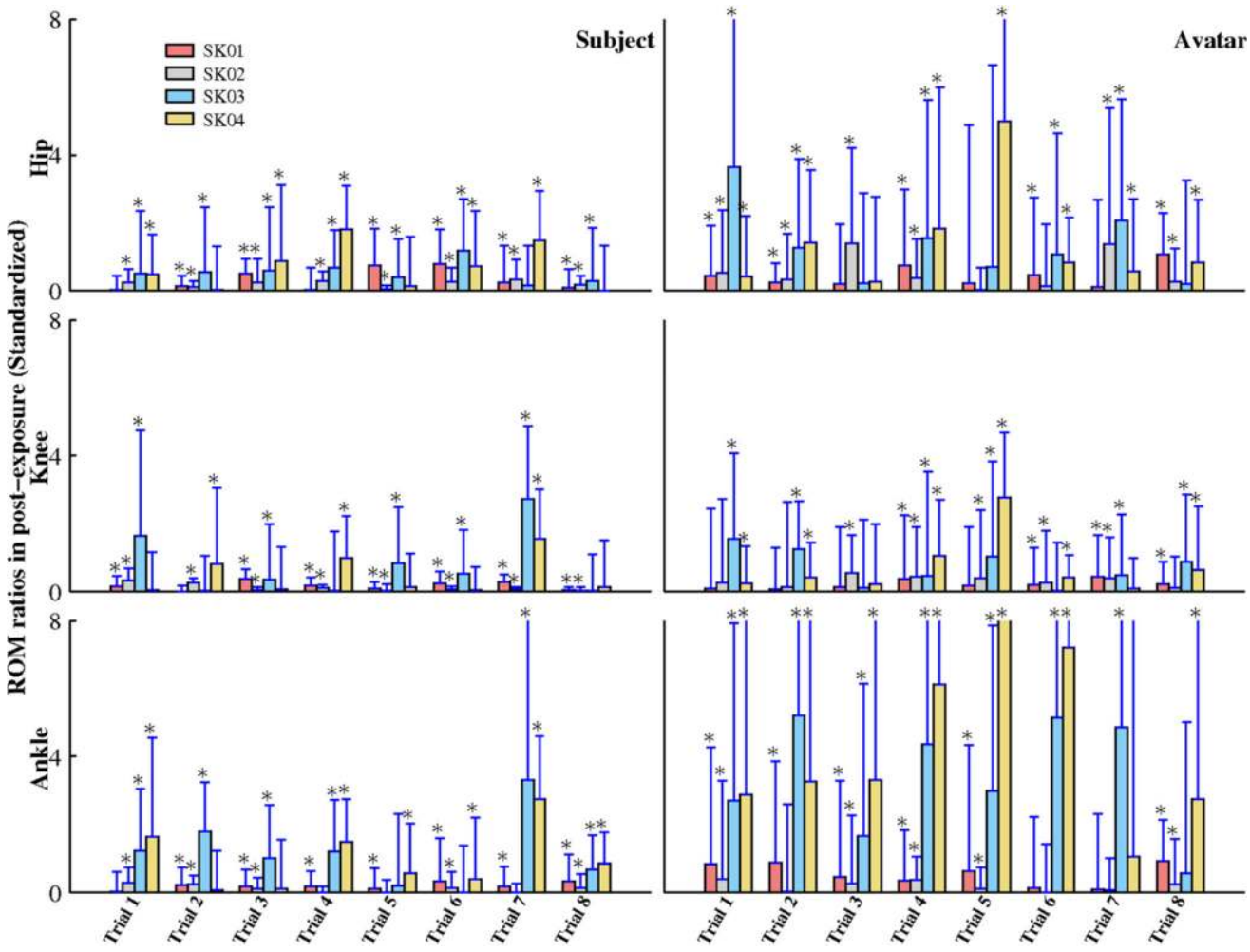

Figure 5.

Range of Motion (ROM) ratios between right and left lower limb joints during visual kinematic perturbation. ROM ratios in post-exposure were standardized (baseline: early-exposure phase). * $P < 0.05$.

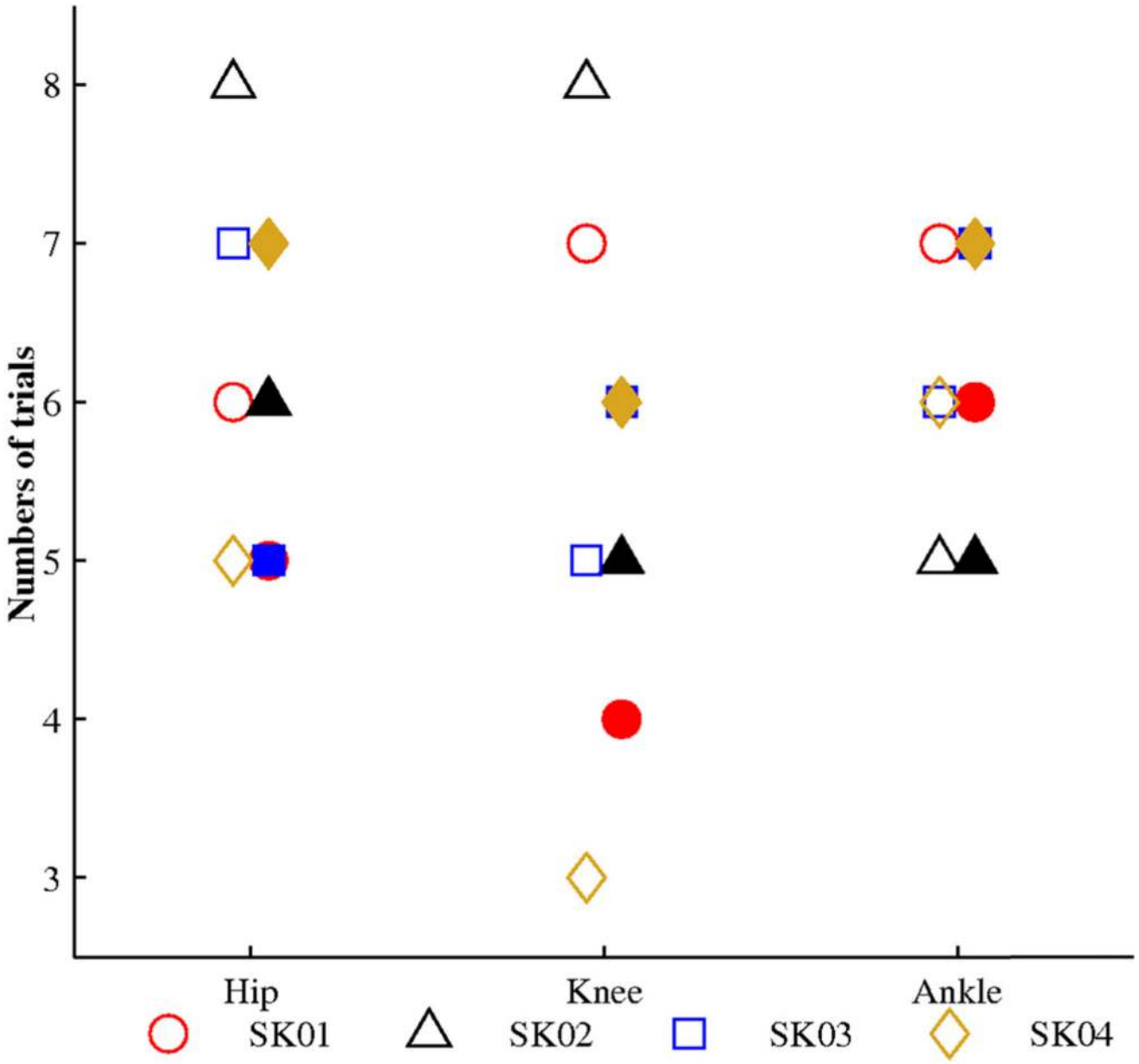

Figure 6.
Numbers of sessions with gait symmetry indexes affected by visual kinematic perturbation. Markers and filled markers represent different subjects and avatar, respectively.

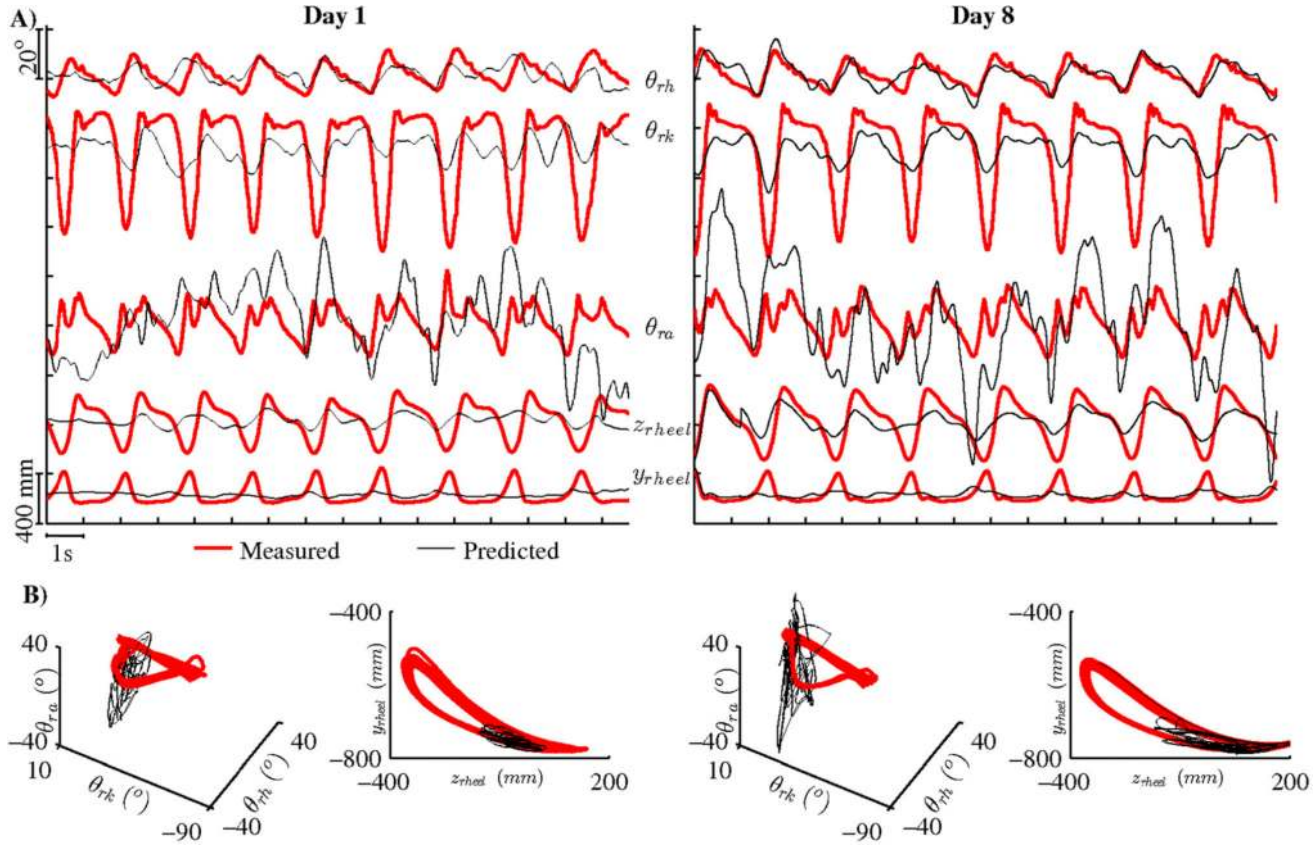

Figure 7.

(a) Reconstructed right leg kinematics from EEG signals in real time for subject SK04 in Day 1 and Day 8. Rows represent hip, knee, and ankle joint angles (θ_{rh}, θ_{rk} and θ_{ra}) and heel positions (calculated from lower limb joint angles). (b) 3D trajectories of lower limb joint angles and heel position portrait.

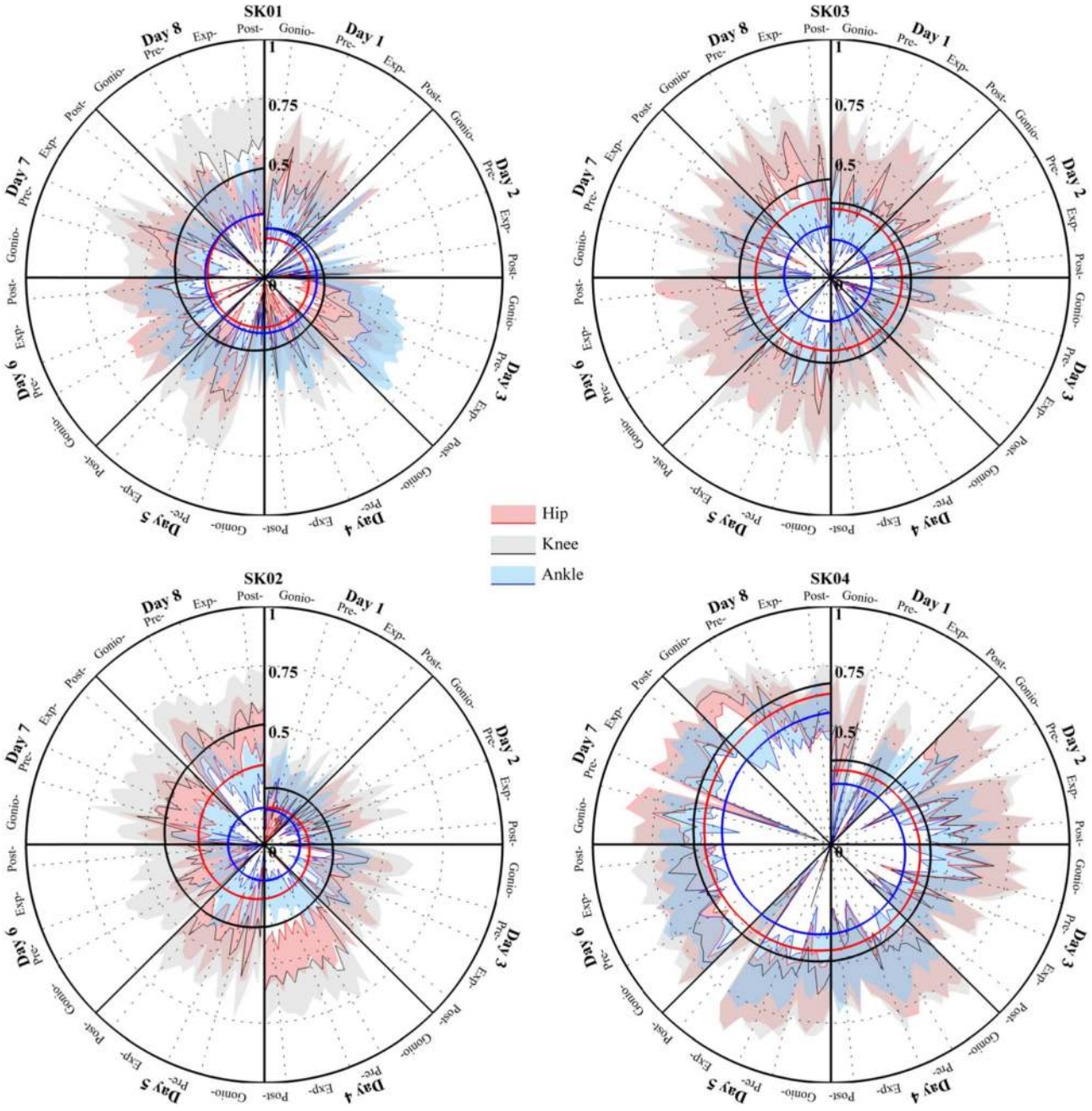

Figure 8.

Pearson's r-values between predicted and actual lower limb joint angles (hip, knee, and ankle) for 4 subjects across 8 days. The shaded areas indicate mean and one standard deviation of r-values. Solid lines are exponential fit for all data points. Dotted lines separate different phases in each day (*gonio-control*, pre-exposure, exposure and post-exposure).

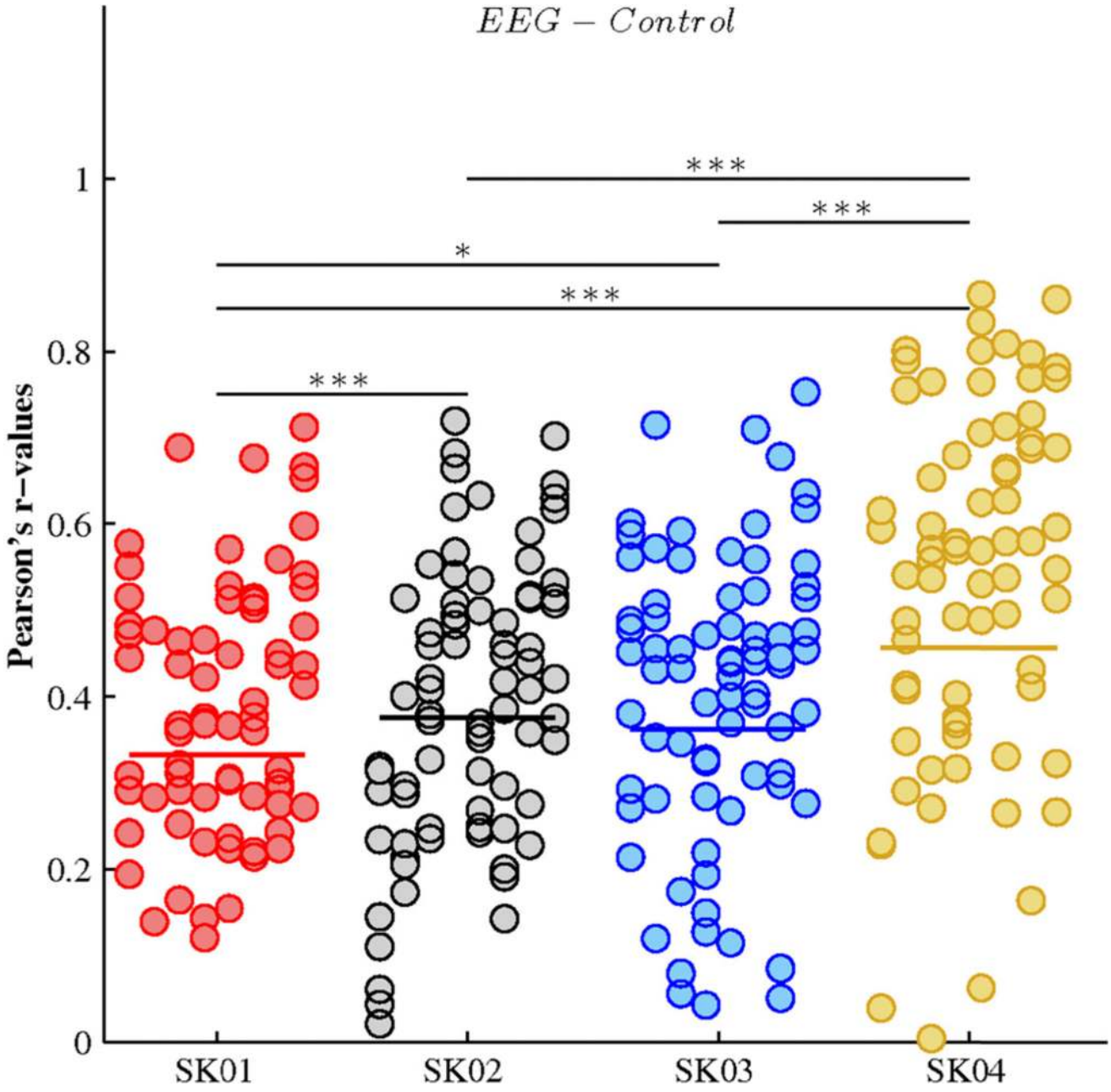

Figure 9.

Pearson's r-values in EEG-control phase for 4 subjects and statistical analysis between subjects using pairwise *t*-test with Tukey-Kramer adjustment. Bars represent the subject's mean. * P<0.05 and *** P<0.001

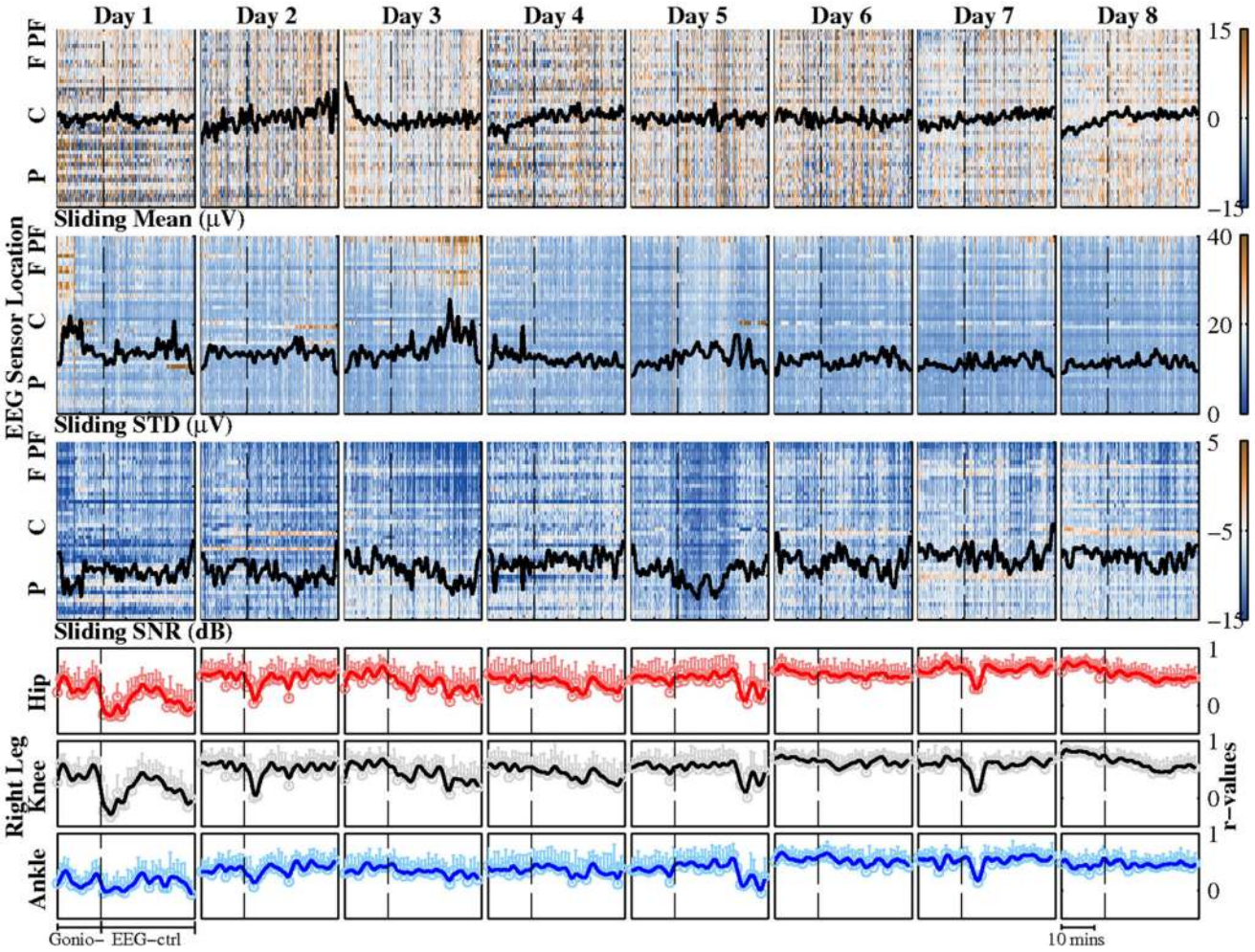

Figure 10.

EEG signals (Mean, STD, and signal to noise ratio (SNR)) and Pearson's r-values for subject SK04 across 8 days. The values were calculated from sliding windows (window size: 5s, and step size of 0.5s). Superimposed bold lines correspond to mean data for all channels. EEG channels are grouped into Pre-Frontal (PF), Frontal (F), Central (C), and Parietal (P) location. Broken lines divide each session into *Gonio-control* (Gonio-) and *EEG-control* (EEG-ctrl) phases.

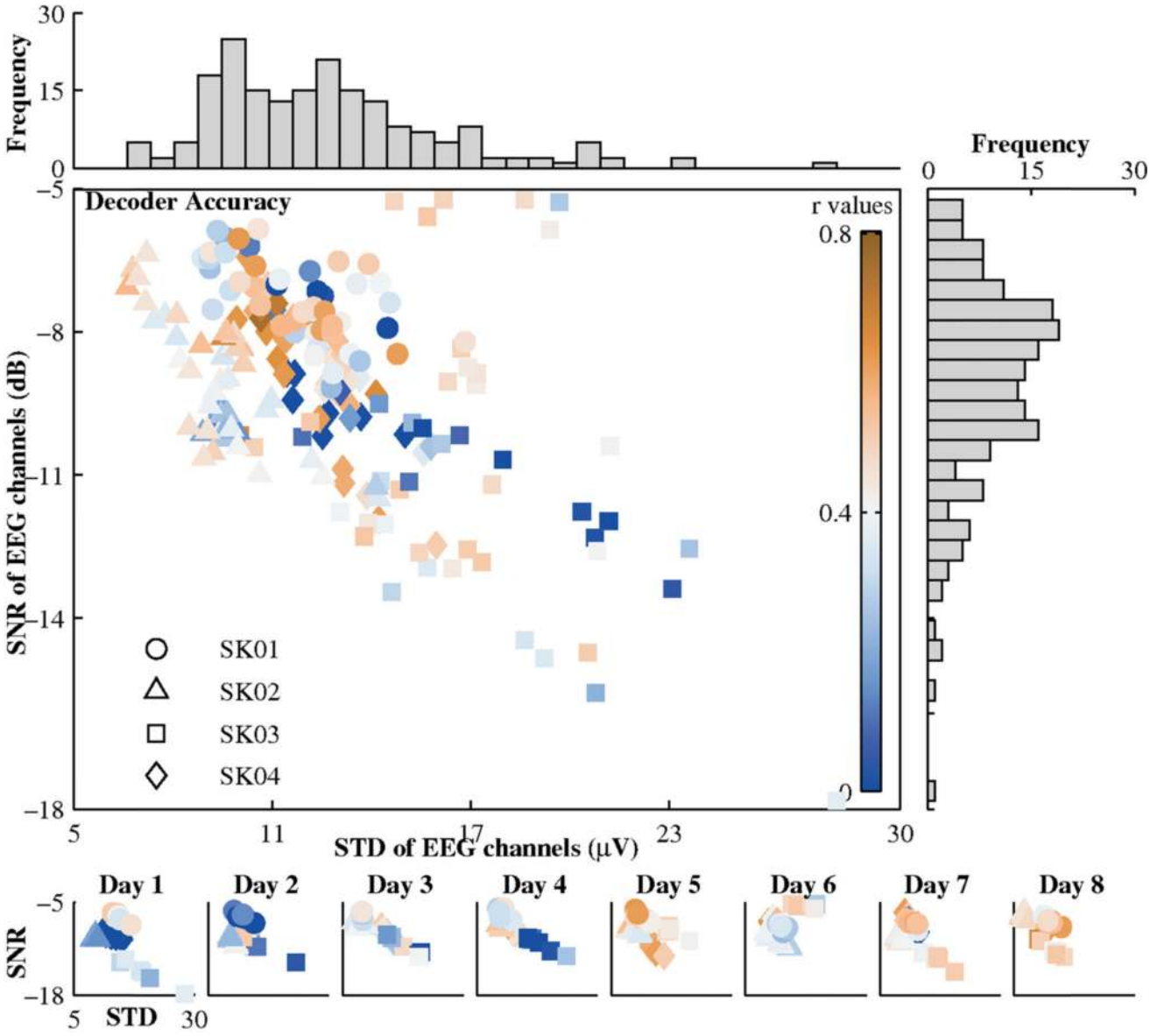

Figure 11.

Pearson's r-values (knee joint) in pre-exposure phase against STD and SNR of EEG signals for 4 subjects across 8 days. Histogram of STD and SNR of EEG signals are showed as bar plot. Pearson's r values for each day are also illustrated.

Table 1

Pearson's r-values for 4 subjects on Day 1 and Day 8

		SK01	SK02	SK03	SK04
Hip	Day 1	0.33 ± 0.23	0.10 ± 0.22	0.36 ± 0.26	0.31 ± 0.31
	Day 8	0.29 ± 0.25	0.38 ± 0.25	0.38 ± 0.27	0.72 ± 0.12
Knee	Day 1	0.37 ± 0.22	0.21 ± 0.22	0.36 ± 0.30	0.41 ± 0.26
	Day 8	0.44 ± 0.21	0.53 ± 0.21	0.45 ± 0.25	0.81 ± 0.08
Ankle	Day 1	0.18 ± 0.21	0.16 ± 0.19	0.16 ± 0.24	0.16 ± 0.25
	Day 8	0.25 ± 0.21	0.31 ± 0.21	0.20 ± 0.18	0.45 ± 0.20

Values are mean ± standard deviation (STD).